Building and Environment 119 (2017) 153–168

Contents lists available at ScienceDirect

Building and Environment

journal homepage: www.elsevier.com/locate/buildenv

New generalized expressions for forced convective heat transfer coefficients at building facades and roofs

H. Montazeri [a, b, *], B. Blocken [a, b]

[a] Building Physics Section, Department of Civil Engineering, KU Leuven, Kasteelpark Arenberg 40 – bus 2447, 3001 Leuven, Belgium
[b] Building Physics and Services, Department of the Built Environment, Eindhoven University of Technology, P.O. box 513, 5600 MB Eindhoven, The Netherlands

ARTICLE INFO

Article history:
Received 26 November 2016
Received in revised form
10 April 2017
Accepted 18 April 2017
Available online 19 April 2017

Keywords:
Convective heat transfer coefficient
Computational Fluid Dynamics (CFD)
Building Energy Simulation (BES)
Building aerodynamics
Forced convection

ABSTRACT

Previous research indicated that the surface-averaged forced convective heat transfer coefficient (CHTC) at a windward building facade can vary substantially as a function of building width and height. However, existing CHTC expressions generally do not consider the building dimensions as parameters and are therefore strictly only applicable for the building geometry for which they were derived. Most CHTC expressions also categorize facades only as either windward or leeward. This indicates the need for new and more generally applicable CHTC expressions. This paper presents new generalized expressions for surface-averaged forced CHTC at building facades and roofs that contain the reference wind speed, the width and the height of the windward building facade as parameters. These expressions are derived from CFD simulations of wind flow and forced convective heat transfer for 81 different isolated buildings. The 3D Reynolds-averaged Navier-Stokes equations are solved with a combination of the high-Re number realizable k-ε model and the low-Re number Wolfshtein model. First, a validation study is performed with wind-tunnel measurements of surface temperature for a reduced-scale cubic model. Next, the actual simulations are performed on a high-resolution grid with a minimum near-wall cell size of 400 μm to resolve the entire boundary layer, including the viscous sublayer and the buffer layer, which dominate the convective surface resistance. The new CHTC expressions are analytical formulae (trivariate polynomials) that can easily be implemented in Building Energy Simulation (BES) and Building Envelope Heat-Air-Moisture (BE-HAM) transfer programs. The accuracy of the expressions is confirmed by in-sample and out-of-sample evaluations.

1. Introduction

Wind flow around buildings is very complex, as it is characterized by flow impingement, separation, recirculation, reattachment and von Karman vortex shedding in the wake (Fig. 1). This complexity also governs the exterior forced convective heat transfer coefficient (CHTC) at the building surfaces. Knowledge of the CHTC is essential for research and practice in building energy and building component durability [3,4]. It is known that using inappropriate CHTC expressions can lead to considerable errors in Building Energy Simulation (BES) [4] and Building Envelope Heat-Air-Moisture (BE-HAM) transfer simulations [5–9]. Values for the CHTC can be obtained either directly, by so-called primary sources such as measurements and numerical simulations, or indirectly, by secondary sources, in which case these sources have been derived from primary sources.

Direct assessment of the CHTC at building facades and roofs can be performed using either of three methods: on-site measurements (e.g. Refs. [10–14]), wind-tunnel experiments (e.g. Refs. [15–20]) or numerical simulation with Computational Fluid Dynamics (CFD) (e.g. Refs. [21–28]). Each approach has particular advantages and disadvantages. The main advantage of on-site measurements is that they allow capturing the full complexity of the problem under study. However, on-site measurements of CHTC that are often based on the one-dimensional energy balance for the building envelope surface [29] are generally only performed in a limited number of points in space and time [30]. Most on-site measurements of CHTC were performed using one or a few heated plates installed at the facades of a building [10–14]. Another well-known

* Corresponding author. Building Physics Section, Department of Civil Engineering, KU Leuven, Leuven, Belgium.
E-mail address: hamid.montazeri@kuleuven.be (H. Montazeri).

http://dx.doi.org/10.1016/j.buildenv.2017.04.012

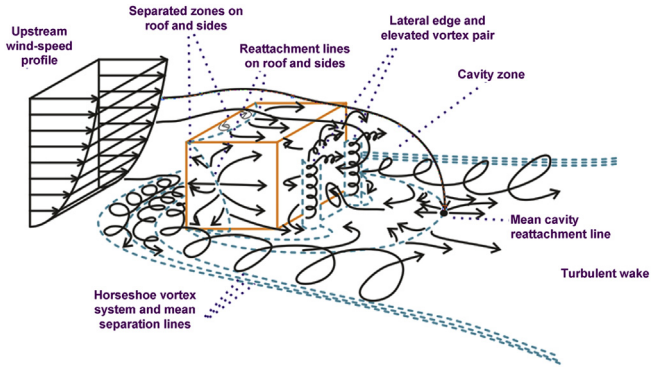

Fig. 1. Schematic illustration of the complexity of wind flow around an isolated rectangular low-rise building ([1] as modified by Ref. [2]).

problem of on-site measurements is that there is no or only very limited control over the boundary conditions such as the meteorological parameters (wind speed, wind direction, temperature, relative humidity, insolation, cloudiness). Wind-tunnel measurements allow a strong degree of control over the boundary conditions. Most available high-resolution wind-tunnel data of CHTC were obtained from measurements either on flat plates parallel or inclined to the approaching flow [15,16] or on bluff bodies, mostly cubes, at relatively low Reynolds numbers (10^3-10^4) and thin turbulent boundary layers [17–20]. Wind-tunnel experiments for flat plates could be considered as full-scale experiments performed on plates in their full dimensions. However, the flow structure around buildings is more complex than the one over flat plates, which casts doubt on the validity of expressions from flat-plate experiments for building applications. Wind-tunnel experiments for small wall-mounted obstacles could be used to obtain information for building applications, but then these wind-tunnel experiments are clearly reduced-scale experiments, where the building model can be at scale 1/20, 1/50 or smaller [18–20]. Due to the much lower Reynolds numbers than in reality ($Re = 10^5$-10^7) they can suffer from the inability to adhere to similarity requirements, which can also limit the applicability of the resulting data for building applications. Numerical simulation with CFD allows either to alleviate or to remove a number of the aforementioned limitations. CFD can provide whole-flow field data, i.e. data on the relevant parameters in all points of the computational domain. Unlike reduced-scale wind-tunnel testing, CFD does not suffer from potentially incompatible similarity requirements because simulations can be conducted at full scale. CFD simulations also easily allow parametric studies. However, the accuracy and reliability of CFD simulations should be ensured by verification, validation and adherence to best practice guidelines [31–36]. Because of these advantages, the use of CFD has rapidly increased in the field of computational wind engineering (CWE) throughout the past 50 years, as highlighted by several recent and not so recent review papers [2,37–47].

CWE also encompasses studies of convective heat transfer on building surfaces. CWE applied to buildings is considered difficult and challenging because of the specific difficulties associated with the flow field around bluff bodies with sharp edges, many of which are not encountered in CFD computations for simple flows such as channel flow and simple shear flow (see e.g. Refs. [37,40,48,49]). Murakami [40] meticulously outlined the main difficulties in CWE: (1) the high Reynolds numbers in wind engineering applications, necessitating high grid resolutions, especially in near-wall regions as well as accurate wall functions; (2) the complex nature of the 3D flow field with impingement, separation and vortex shedding; (3) the numerical difficulties associated with flow at sharp corners and consequences for discretization schemes; and (4) the inflow (and outflow) boundary conditions. Concerning the accurate and reliable CFD simulation of CHTC, the first difficulty is strongly amplified, because of the necessity to resolve the entire thermal boundary layer at all building surfaces, including the very thin viscous sublayer and the buffer layer, which dominate the convective surface resistance. This requires a y^* value smaller than 5 and preferably equal to 1 [50,51] which implies a very high near-wall grid resolution, yielding wall-adjacent cell sizes that can go down to 300 μm [22,23]. Note that the dimensionless wall distance y^* is defined as $u^* y_P / \nu$, where y_P is the distance from the center point P of the wall-adjacent cell to the wall, ν is the kinematic viscosity, and u^* is the friction velocity based on the turbulent kinetic energy k_P in the wall-adjacent cell center point P and on the constant C_μ ($u^* = C_\mu^{0.5} k_p^{0.25}$). Given the typical length scale of buildings (1–100 m) let alone that of cities (1–10 km), it is clear that accurately resolving all thermal boundary layers at building surfaces in an urban area is very challenging, both in terms of ensuring grid quality and grid economy. It should be noted that some authors have resorted to the development of adjusted temperature wall functions [52–54], which is a promising approach, but this approach needs to be investigated further before it can be applied with confidence for various types of buildings.

Because of the complexities and expenses involved in obtaining accurate CHTC information using the direct approach by measurement or simulations, the indirect approach is often pursued. This refers to the use of analytical expressions (often called "correlations") that have been established mostly based on previous on-site measurements or wind-tunnel measurements or on CFD simulations. Many of these expressions are implemented in Building Energy Simulation (BES) programs [3,4,55] and BE-HAM (Buildings Envelope Heat, Air an Moisture transfer) computational codes [5,7,56–58]. Comprehensive reviews on these expressions were presented by Palyvos [3] and Mirsadeghi et al. [4]. Although a wide range of such expressions exists, there are a few main shortcomings that most have in common, and which are described below. This discussion will be limited to forced convective heat transfer.

A first main shortcoming is that existing (forced) CHTC expressions focus on wind speed as the main (or only) parameter and do not consider the building dimensions or surface width and length as parameters. To the best of our knowledge, the only exception is the BLAST detailed convection expression in which the surface perimeter and surface area are included, mainly from the perspective of boundary layer development over a flat plate [59,60]. This inherently implies that every expression (except BLAST) is strictly only applicable for the building geometry (and other conditions) for which it was established. This implication would not be very important if the influence of building geometry on the forced CHTC statement would be limited. However, recent CFD research for a wide range of building geometries [28] has shown that this influence can be very large and to some extent counter-intuitive, as shown in Fig. 2. For example, for a 10 m wide windward facade, increasing the height from 10 m to 80 m increases the forced surface-averaged CHTC on the windward facade by about 20% (Fig. 2a). However, for H = 10 m, increasing the building width from 10 to 80 m has the opposite impact on the forced surface-averaged CHTC, which decreases by more than 33% (Fig. 2b). The first trend can be explained by the increase of wind speed with height in the atmospheric boundary layer. The second is attributed to the so-called wind-blocking effect. This effect was first defined in 2006 [61] and refers to the upstream wind deceleration due to the blockage by the building. The higher and wider the building, the stronger the wind-blocking effect, and the larger the upstream wind deceleration [28,62–64]. To the best knowledge of the

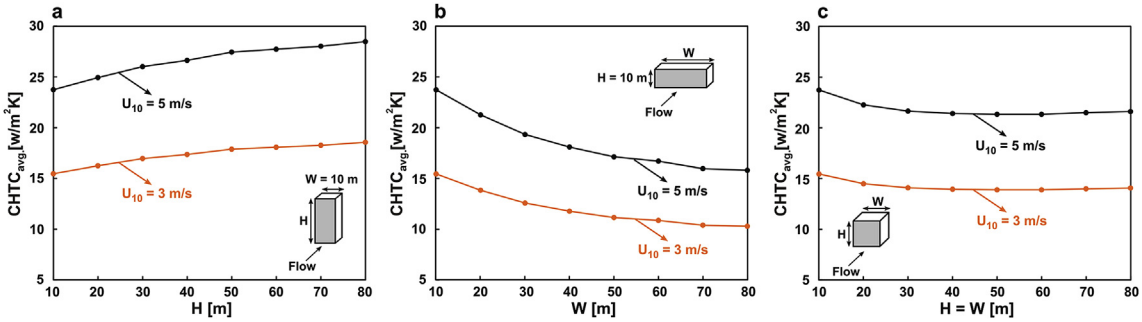

Fig. 2. Profile of surface-averaged CHTC/($U_{10}^{0.84}$) on the windward facade of buildings with (a) W = 10 m and different values of H, (b) H = 10 m and different values of W, and (c) H = W [28].

authors, these geometry effects have not yet been implemented in any CHTC expression. The trend in Fig. 2c, for buildings with a square windward surface, is a result of both facts combined (increase of wind speed with height and wind-blocking effect).

A second main shortcoming is that most existing CHTC expressions only consider building facades and not building roofs. In addition, facades are generally only classified as either windward or leeward, while flow structures on the side facades and the back (leeward) facade are clearly very different, as shown in Fig. 1. The two main shortcomings indicate the need for new and more generally applicable CHTC expressions, for building facades and roofs, in which the building dimensions are present as parameters.

This paper presents new generalized expressions for surface-averaged forced CHTC at building facades and roofs that contain the reference wind speed, the width and the height of the windward building facade as parameters. The new expressions are analytical formulae that can be easily implemented in Building Energy Simulation (BES) and Building Envelope Heat-Air-Moisture (BE-HAM) transfer programs. First, a validation study is conducted based on wind-tunnel measurements of wind flow and surface temperature for a reduced-scale cubic model. Next, the actual simulations are performed for 81 different isolated buildings. The 3D steady Reynolds-averaged Navier-Stokes (RANS) equations are solved with a combination of the high-Re number realizable k-ε model and the low-Re number Wolfshtein model. The simulations are performed on a high-resolution grid resulting from grid-sensitivity analysis and with a minimum near-wall cell size of 400 μm to resolve the entire boundary layer, including the viscous sublayer and the buffer layer, which dominate the convective surface resistance. Finally, the multivariate polynomial interpolation technique is used to derive the new expressions from the CFD results.

This paper contains six sections. In Section 2, the CFD validation study is outlined. Section 3 describes the CFD simulations for the full-scale buildings. Section 4 presents the CFD results and the resulting new CHTC expressions. In Section 5, a discussion on the limitations of the study is given. The main conclusions are presented in Section 6.

2. CFD validation study

The CFD validation was reported in an earlier publication [28]. However, because of its importance for the present paper, a summary is provided below.

2.1. Wind-tunnel experiments

Meinders et al. [19,65] analyzed convective heat transfer at the surfaces of a cube in turbulent channel flow. The channel had a height of 0.05 m and a width of 0.6 m. The approach flow had a constant air temperature of 21 °C. The cube had a height (H_c) of 0.015 m resulting in a blockage ratio in the channel of 0.75%. The cube had a copper core ($12 \times 12 \times 12$ mm^3) around which an epoxy layer of 0.0015 m was applied on all surfaces. This core was heated at a constant temperature of 75 °C by a resistance wire inside the core. Due to the high thermal conductivity of the copper, a uniformly distributed temperature at the interior of the epoxy layer was obtained. Experiments were performed under perpendicular approach flow and for several Reynolds numbers (based on H_c) ranging from 2000 to 5000. In the present study, only Re = 4440 is considered. The approach-flow turbulent boundary layer mean velocity and turbulent kinetic energy were obtained by laser-Doppler anemometry. The external surface temperature distribution of the epoxy cube surface was measured with infrared thermography. Meinders et al. [19,65] used the Finite Volume Method to solve the equation for the three-dimensional heat conduction problem for the epoxy layer to obtain the local convective heat transfer coefficient.

2.2. CFD simulation and validation

The computational geometry includes the cube with its epoxy layer (Fig. 3). The upstream and downstream domain lengths are $4H_c$ = 0.06 m and $10H_c$ = 0.15 m, respectively. Note that the upstream length is smaller than proposed by best practice guidelines [33,34], to limit unintended streamwise gradients in the inlet profiles [66,67]. The domain height is chosen equal to that of the channel in the experiments (= $3.3H_c$). The computational grid is generated with the surface-grid extrusion technique [68]. 40 cells with a uniform grid spacing (i.e. stretching ratio = 1) are applied along the cube edges (with 4 cells across the epoxy layer thickness) (Fig. 4). The cubical cells extend up to a distance of $H_c/3$ from the cube surfaces. Beyond this distance, a stretching factor of 1.05 is applied, to limit the total number of cells, resulting in a total of 2,180,960 hexahedral cells. The grid resolution results from a grid-sensitivity analysis (not outlined in this paper). The distance from the center point of the wall-adjacent cell to the wall is $y_P = 1.88 \times 10^{-4}$ m, corresponding to an average y^* value of 3.8 over the cube surfaces. The maximum y^* value of 6.9 only occurs at the top corners of the windward surface. Planes with labels "1" and "3" in Fig. 3a are the inlet and outlet planes, while planes with labels "2" and "4" are the side planes. The inlet velocity profile needed for the CFD simulations is not given in Ref. [19] but was obtained by Montazeri et al. [28] and shown in Fig. 5 for mean wind speed U and turbulent kinetic energy k. The turbulence dissipation rate $\varepsilon = u^{*3}/(\kappa(z + z_0))$ with u^* the friction velocity (= 0.25 m/s), κ the von Karman constant (= 0.42) and z_0 the aerodynamic roughness length based on a fit with the measured mean wind speed profile ($= 7.6 \times 10^{-6}$ m).

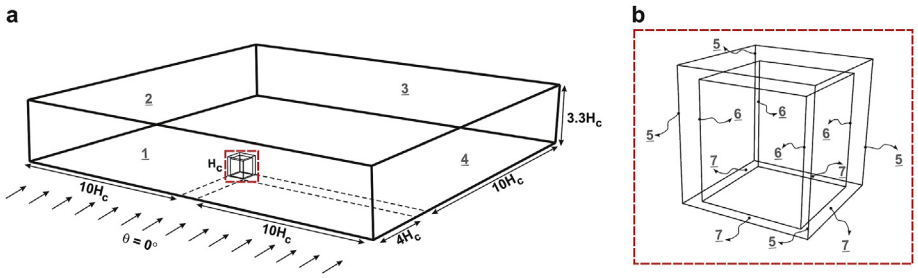

Fig. 3. Perspective view of computational domain and cube including epoxy layer, with numbers referring to boundary condition types.

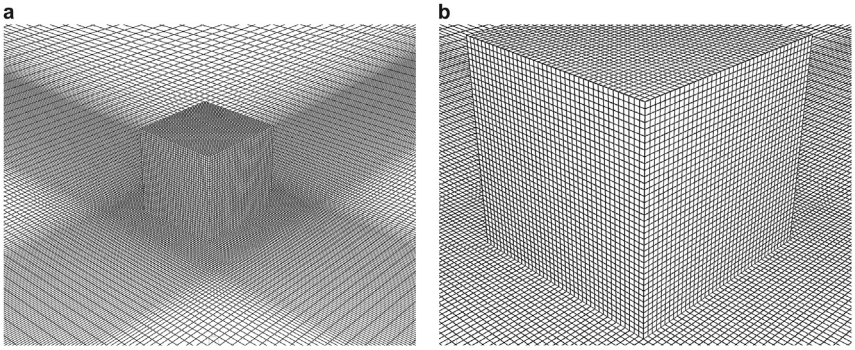

Fig. 4. High-resolution computational grid at cube surfaces and part of the ground surface (total number of cells: 2,180,960).

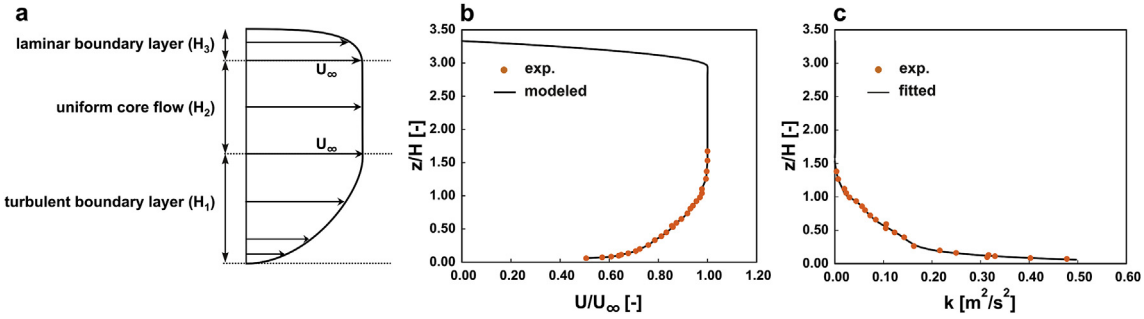

Fig. 5. (a) Schematic and (b) measured (dots) and modeled (solid line) vertical profile of normalized mean wind speed. (c) Measured (dots) and modeled (solid line) vertical profile of turbulent kinetic energy.

Zero static pressure is applied at the outlet plane. Symmetry conditions, i.e. zero normal velocity and zero normal gradients of all variables, are applied at the lateral sides of the domain. The ground and top of the domain are defined as no-slip smooth walls. The thermal boundary conditions are a uniform inlet air temperature of 294 K (21 °C) and a fixed surface temperature of 348 K (75 °C) for the inner surface of the epoxy layer (planes with label "6" in Fig. 3b). To couple the two zones on the solid/fluid interface (planes with label "5" in Fig. 3b), heat transfer is calculated directly from the solution of temperature in the adjacent cells of the fluid (air) and solid (epoxy layer). For the bottom of the epoxy layer (planes with label "7" in Fig. 3b), the average value of the surface temperature of the windward surface close to the ground plane ($H_c/65$) and the copper core is used. The bottom and top surfaces of the computational domain are adiabatic walls.

The 3D steady RANS equations are solved with the commercial CFD code Ansys/Fluent 12.1 [69]. The high-Re number realizable k-ε model (Rk-ε) [70] is used in combination with the low-Re number Wolfshtein model [71] for closure. The relative importance of buoyancy effects is assumed negligible as the ratio of the Grashof number to the Reynolds number squared (Gr/Re^2) is smaller than 0.3 [65]. Therefore, only forced convection is considered. Note that because of the relatively high temperature difference between the cube surfaces and the surroundings, radiative heat transfer has also occurred in the measurements. In order to investigate the contribution of the radiative heat flux compared to the convective heat flux, the following analysis is performed. The radiation in the measurement can be simplified by the Stefan Boltzmann law, i.e. $Q''_{rad} = \varepsilon\sigma\left(T^4_{surf} - T^4_{amb}\right)$, where ε is the surface emissivity of the cube (= 0.95), σ the Stefan Boltzmann constant (= 5.67×10^{-8} W/m^2K^4), T_{sur} the surface temperature and T_{amb} the ambient temperature (= 21 °C). The conductive heat flux can be approximated with the one-dimensional Fourier law, i.e. $Q''_{cond} = \lambda\left(T_{co} - T_{surf}\right)/L$, where λ is the thermal conductivity of the epoxy (= 0.24 W/mK), T_{co} the copper temperature (= 75 °C) and L the epoxy layer thickness. A heat balance at the surface yields the local convective heat flux,

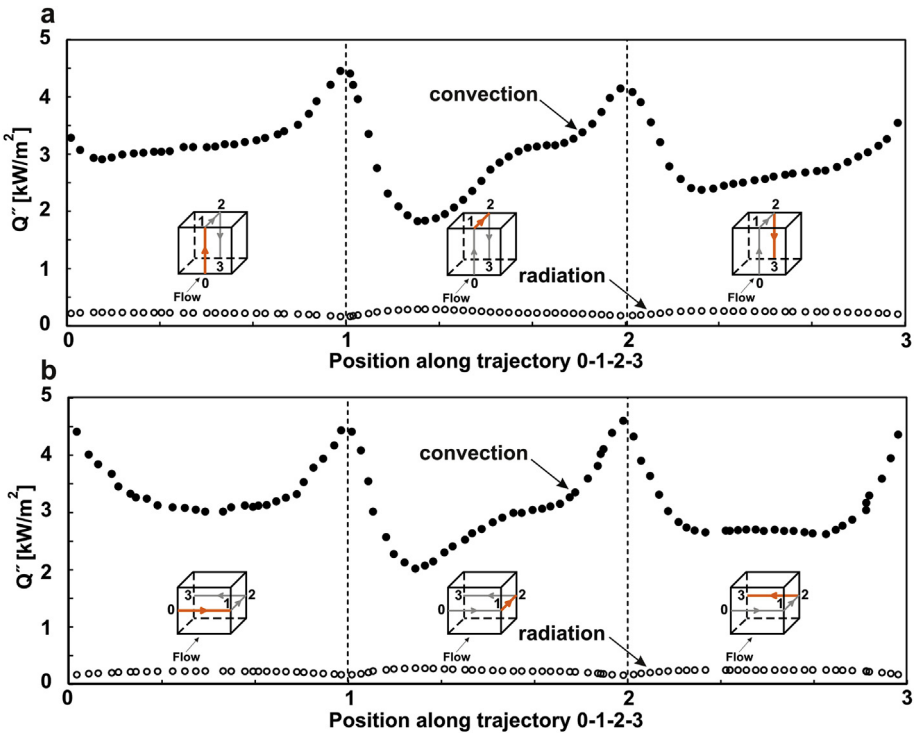

Fig. 6. Comparison of radiative heat flux and convective heat flux along trajectory 0-1-2-3 on the cube surfaces.

$Q''_{conv} = Q''_{cond} - Q''_{rad}$. Using the measured surface temperatures, the local convection and radiation heat transfer can be estimated along lines for which the experimental data are available. The results are shown in Fig. 6. It can be observed that the convective heat fluxes were much larger than radiative heat fluxes. This was also pointed out by Meinders et al. [19,65]. Therefore, in the present study, radiation is not taken into account.

The SIMPLE algorithm is used for pressure-velocity coupling, pressure interpolation is second order and second-order discretization schemes are used for both the convection terms and the

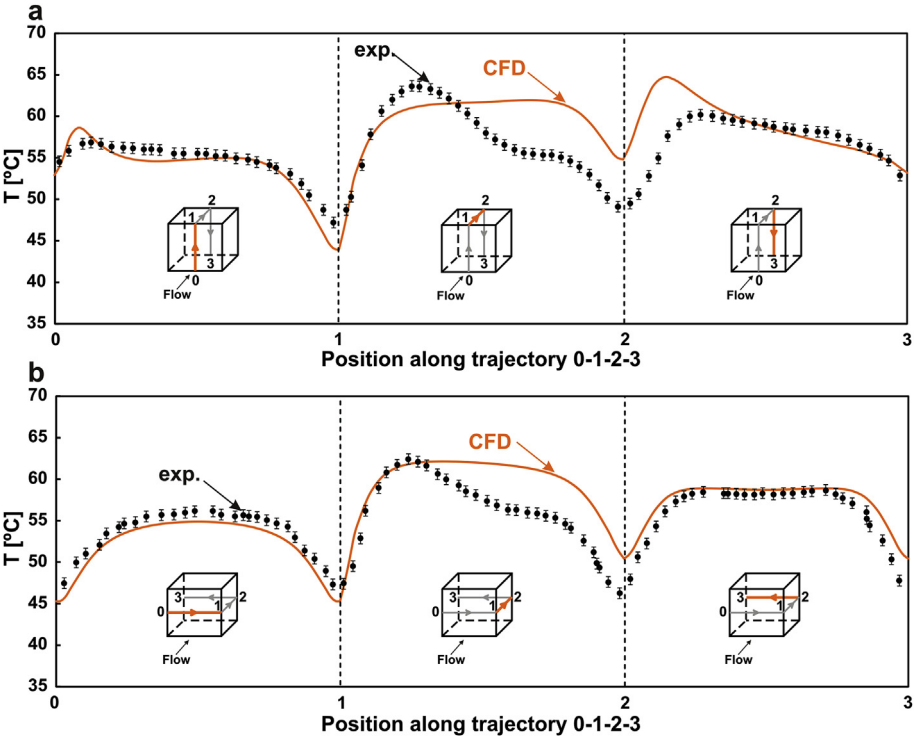

Fig. 7. Comparison of simulated and measured surface temperature along trajectory 0-1-2-3 on the cube surfaces.

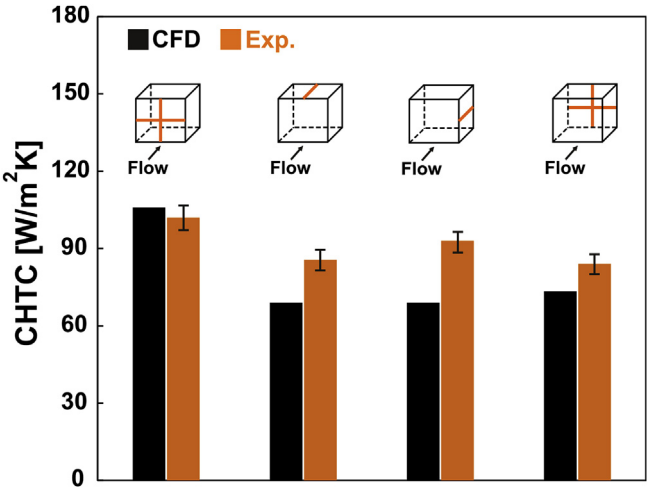

Fig. 8. Comparison of simulated and measured convective heat transfer coefficient (CHTC) averaged along lines on the cube surfaces.

viscous terms of the governing equations. Convergence is declared when all the scaled residuals level off and reach the values 10^{-7} for x, y, z momentum and energy, 10^{-5} for continuity and 10^{-6} for k and ε.

Fig. 7a and b compare the experimental and CFD results of surface temperature along lines in a vertical and horizontal mid-plane, and Fig. 8 compares experimental and numerical CHTC averaged along the lines for which data were available. For the windward surface, the general agreement is good with average deviations of about 1.7 and 2.4% along the vertical and horizontal lines, respectively, in spite of some overestimation close to the ground (Fig. 7a). This could be due to (1) additional heat loss of the epoxy layer through the base wall in the experiment which is not taken into account in the simulations and/or (2) incorrect prediction of the size and shape of the standing vortex due to the upstream longitudinal gradients in the approach-flow profiles [66,67]. Less good agreement is present at the top and side surfaces of the cube with average deviations in excess of 6.5 and 6.6%. These deviations are attributed to the well-documented inaccurate flow field prediction by steady RANS downstream of the windward facade [45,72–74]. Nevertheless, for the leeward surface, CFD shows a good performance along the horizontal line, especially in the middle of the line. Close to the side edges, however, overestimations occur. A large overestimation occurs close to the upper edge of the leeward surface (along the vertical line), which is probably due to intermittent reattachment of the flow near the downwind roof edge and the related flow behavior near this upper edge. Driven by the good agreements between CFD and wind-tunnel experiments for the windward and the leeward surface, and to a lesser extent for the top and side surfaces, the computational parameters and settings of the validation study are also used for the study for the full-scale buildings in the next sections. Note that the new CHTC expressions will be derived based on the surface-averaged CHTC values, though the validation study is performed by comparing the experimental and CFD results of surface temperature and CHTC along lines for which the experimental data are available.

3. CFD simulations for 87 full-scale buildings

3.1. List of cases

CFD simulations are performed for 87 different isolated building geometries (81 geometries to establish the CHTC expressions, and 6 geometries to evaluate the out-of-sample accuracy of the expressions). The simulations can be classified into three groups based on their objective (Table 1):

Table 1
Geometry of the 87 building geometries and values of reference wind speed.

Objective	Building geometry	No. of geometries	No. of simulations	Height (m)	Width (m)	Depth (m)	U_{10} (m/s)
GROUP 1: Obtain CHTC-Re correlations	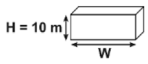	8	32	10	10, 20, 30, 40, 50, 60, 70, 80	20	1, 2, 3, 4
	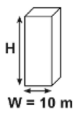	3	12	10, 20, 30	10	20	1, 2, 3, 4
	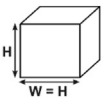	3	12	10, 20, 30	W = H	20	1, 2, 3, 4
GROUP 2: Obtain CHTC-building dimension correlations	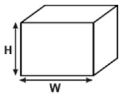	9	9	5	5, 10, 20, 30, 40, 50, 60, 70, 80	20	1
		9	9	10	5, 10, 20, 30, 40, 50, 60, 70, 80	20	1
		9	9	20	5, 10, 20, 30, 40, 50, 60, 70, 80	20	1
		9	9	30	5, 10, 20, 30, 40, 50, 60, 70, 80	20	1
		9	9	40	5, 10, 20, 30, 40, 50, 60, 70, 80	20	1
		9	9	50	5, 10, 20, 30, 40, 50, 60, 70, 80	20	1
		9	9	60	5, 10, 20, 30, 40, 50, 60, 70, 80	20	1
		9	9	70	5, 10, 20, 30, 40, 50, 60, 70, 80	20	1
		9	9	80	5, 10, 20, 30, 40, 50, 60, 70, 80	20	1
GROUP 3: Out-of-sample fit evaluation	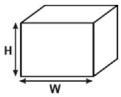	1	5	15	65	20	0.5, 1, 1.5, 2.5, 3.5
		1	5	25	35	20	0.5, 1, 1.5, 2.5, 3.5
		1	5	25	25	20	0.5, 1, 1.5, 2.5, 3.5
		1	5	25	45	20	0.5, 1, 1.5, 2.5, 3.5
		1	5	25	65	20	0.5, 1, 1.5, 2.5, 3.5
		1	5	35	65	20	0.5, 1, 1.5, 2.5, 3.5

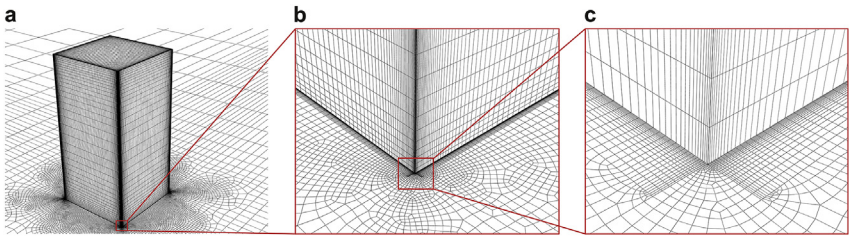

Fig. 9. High-resolution grid at building surfaces and part of the ground surface for building H = 40 m and W = 20 m (total number of cells: 1,911,316).

- Group 1: Simulations to establish the expressions of forced surface-averaged CHTC as a function of reference wind speed U_{10} (or Re). Simulations are made for 12 building geometries and 4 reference wind speeds U_{10} = 1, 2, 3 and 4 m/s.
- Group 2: Simulations to establish the expressions of forced surface-averaged CHTC as a function of width and height of windward facade. Simulations are made for 81 building geometries, all with U_{10} = 1 m/s.
- Group 3: Simulations to evaluate the out-of-sample accuracy of the expressions. Simulations are made for 6 building geometries, and for U_{10} = 0.5, 1, 1.5, 2.5 and 3.5 m/s.

3.2. Computational settings and parameters

The dimensions of the computational domains are chosen based on the best practice guidelines by Franke et al. [33] and Tominaga

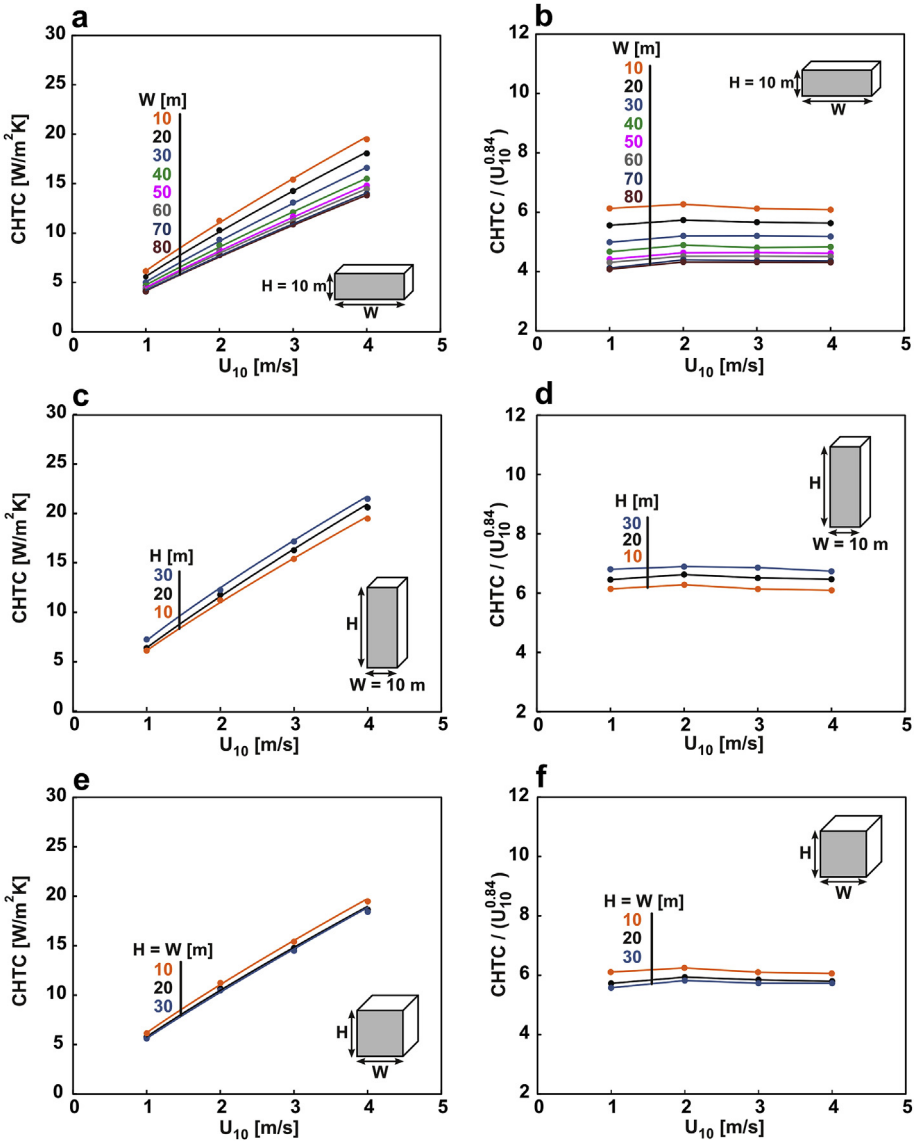

Fig. 10. Forced surface-averaged CHTC on the windward facade as a function of U_{10} for buildings with (a) H ≤ W, (c) H ≥ W and (e) H = W. (b,d,f) Same for ratio $CHTC_{avg}/U_{10}^{0.84}$.

et al. [34]. The upstream and downstream domain length are 5H and 15H, respectively. A high-resolution hybrid grid with 1,911,316 prismatic and hexahedral cells is generated using the surface-grid extrusion technique [68] (Fig. 9). In this case, y_p, the distance from the center point of the wall-adjacent cell to the wall, is about 400 μm. The maximum y^* value is below 5 for all building geometries.

At the inlet of the domain, neutral atmospheric boundary layer inflow profiles of mean wind speed U (m/s), turbulent kinetic energy k (m^2/s^2) and turbulence dissipation rate ε (m^2/s^3) are imposed:

$$U(z) = \frac{u^*_{ABL}}{\kappa} \ln\left(\frac{z + z_0}{z_0}\right) \quad (1)$$

$$k(z) = 1.5(I_U(z)U(z))^2 \quad (2)$$

$$\varepsilon(z) = \frac{u^*}{\kappa(z + z_0)} \quad (3)$$

The wind direction is perpendicular to one of the building facades. The buildings are situated on a large grass-covered terrain with an aerodynamic roughness length $z_0 = 0.03$ m [75]. The reference wind speed at 10 m height, U_{10}, ranges from 1 to 4 m/s, yielding building Re ranging from 0.7×10^6 to 8.5×10^6 based on the building height H. Note that using the relatively low reference wind speed is to avoid a prohibitively high total number of computational cells and the need for excessive computational resources, because the thickness of the boundary layer at the building surfaces decreases with increasing Re. For all simulations, the longitudinal turbulence intensity I_u, that is imposed at the inlet ranges from 20% at ground level with exponential decay to 5% at gradient height. The turbulent kinetic energy k is calculated from U and I_u using Eq. (2) and assuming that the standard deviations of the turbulent fluctuations in the three directions are similar ($\sigma_u = \sigma_v = \sigma_w$). The building and ground surfaces are considered smooth no-slip walls. Zero static pressure is applied at the outlet plane. Symmetry conditions (zero normal velocity and zero gradients) are applied at the top and lateral sides of the domain. The thermal boundary conditions are a uniform inlet air temperature of 10 °C and a fixed surface

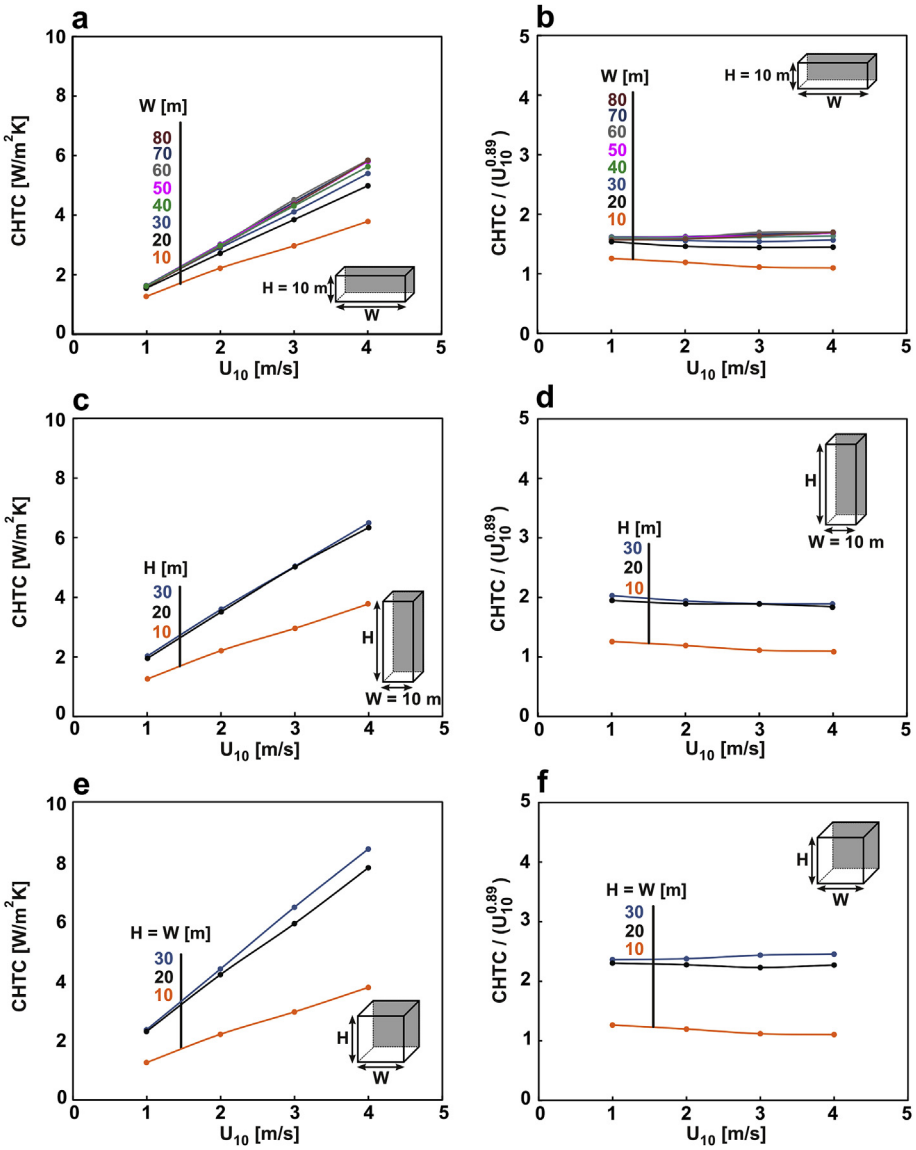

Fig. 11. Forced surface-averaged CHTC on the leeward facade as a function of U_{10} for buildings with (a) H ≤ W, (c) H ≥ W and (e) H = W. (b,d,f) Same for ratio $CHTC_{avg}/U_{10}^{0.89}$.

temperature of 30 °C for the building surfaces. The adiabatic boundary condition is used for the ground surface.

The solver settings are identical to those in the validation study reported in Sec. 2.2. The 3D steady RANS equations with the realizable k-ε turbulence model are solved in combination with the low-Re number Wolfshtein model [71]. The results of the simulations will be reported in the next section along with the establishment of the new expressions.

4. New expressions

4.1. Relationship between CHTC and reference wind speed

The simulations from Group 1 (see above and Table 1) are used to establish the relationship between the forced surface-averaged CHTC and the reference wind speed U_{10}. Fig. 10 summarizes the results of the CFD simulations for the windward facade. Fig. 10a shows the increase of CHTC with increasing U_{10} for buildings with H = 10 m and W ranging from 10 m to 80 m. Based on fitting with power-law functions, the fit with power-law exponent 0.84 yields the best performance for all building geometries (R^2 = 0.9829 to 0.9994). This is also demonstrated in Fig. 10b, where the parameter $CHTC_{avg}/U_{10}^{0.84}$ is plotted versus U_{10}. With exponent 0.84, it appears that the ratio $CHTC_{avg}/U_{10}^{0.84}$ is independent of U_{10}. Similar results are provided in Fig. 10c–d for buildings with W = 10 m and H ranging from 10 to 30 m, and in Fig. 10e–f for buildings with W = H ranging from 10 to 30 m. The power-law relationship with U_{10} is known from previous studies for particular building geometries (e.g. Refs. [21–23,28]). The fact however that the same power-law seems to hold irrespective of building width and height, has to the best of our knowledge not be revealed before.

Figs. 11–13 provide similar CFD simulation results for the leeward facade, the side facade and the roof, respectively. The same observations apply as for the windward facade, although the exponents are slightly different: 0.89 for the leeward facade, 0.88 for the side facade and 0.90 for the roof. However, each of these exponents seems to hold for a wide range of geometries studied, which greatly simplifies the establishment of a generally valid

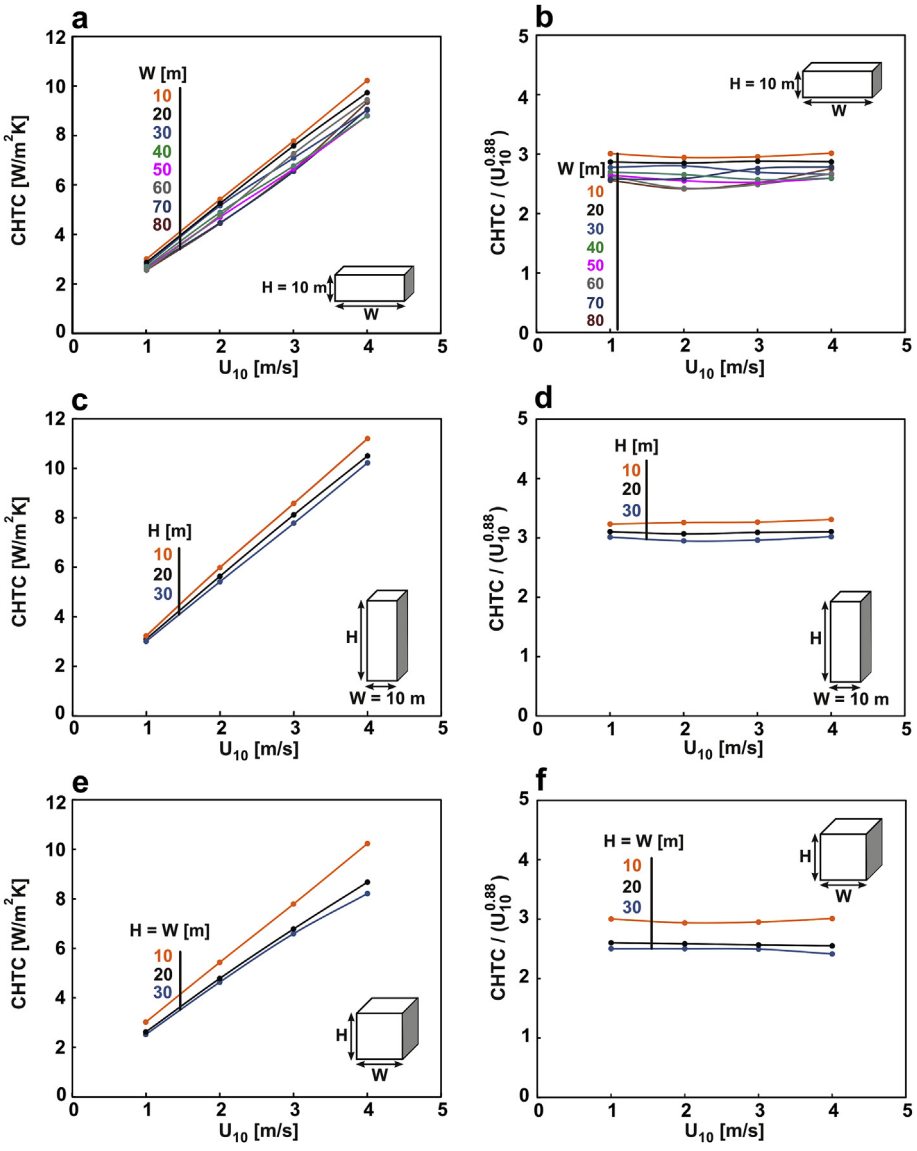

Fig. 12. Forced surface-averaged CHTC on the side facade as a function of U_{10} for buildings with (a) H ≤ W, (c) H ≥ W and (e) H = W. (b,d,f) Same for ratio $CHTC/U_{10}^{0.88}$.

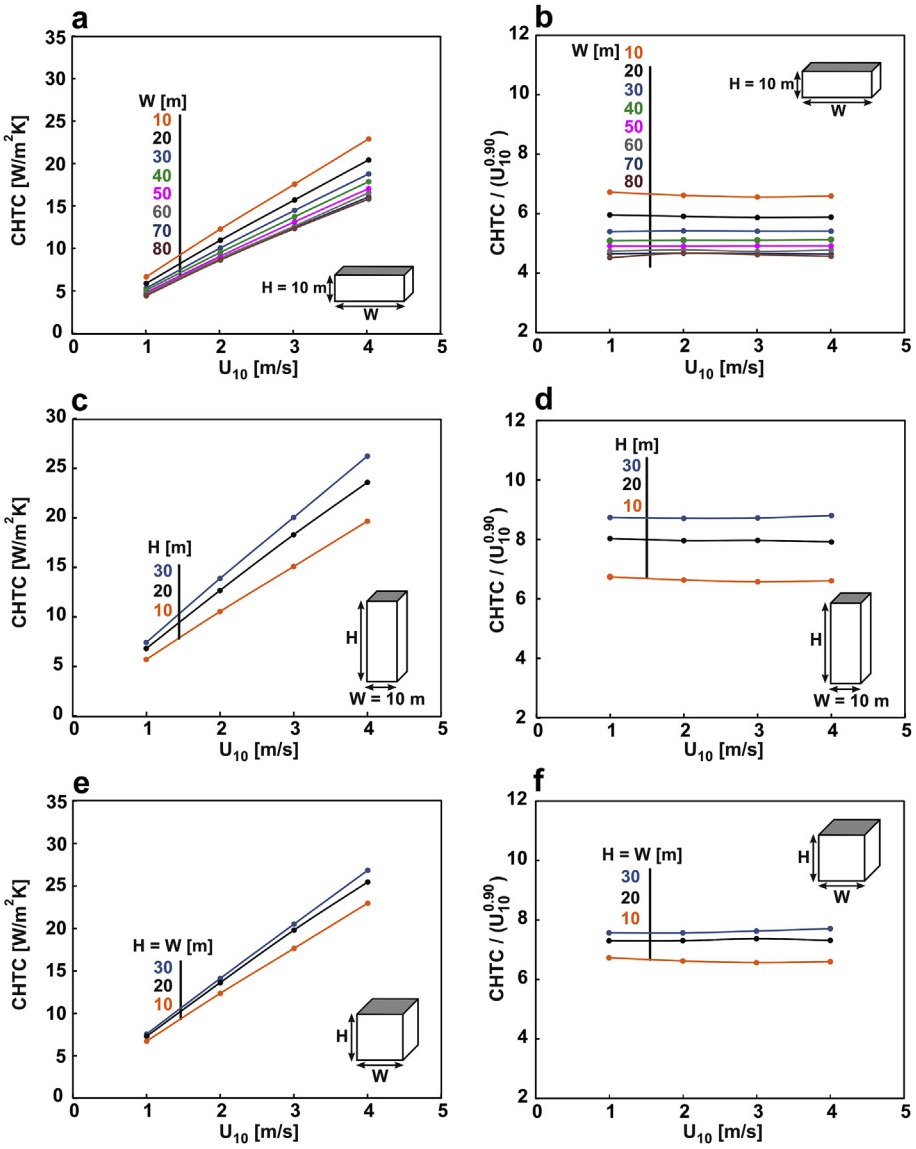

Fig. 13. Forced surface-averaged CHTC on the roof as a function of U_{10} for buildings with (a) H ≤ W, (c) H ≥ W and (e) H = W. (b,d,f) Same for ratio $CHTC_{avg}/U_{10}^{0.90}$.

expression. In addition, it suggests that the establishment of the relationship between CHTC and building width and height should only be performed for a single value of U_{10}. Therefore, this approach is adopted in the next subsection. Afterwards, out-of-sample evaluations will be performed to validate this approach.

4.2. Relationship between CHTC and building width and height

The simulations from Group 2 (see above and Table 1) are used to establish the relationship between the forced surface-averaged CHTC and building width W and height H. As indicated in Table 1, simulations are only performed for $U_{10} = 1$ m/s.

Fig. 14a displays the surface-averaged ratio $CHTC/U_{10}^{0.84}$ as a function of W and H for the windward facade. This plane can be described with good approximation ($R^2 = 0.9977$) by the polynomial in Table 2. Using the coefficients with 2 decimal digits instead of 8 provides a deviation of about 0.19%. Using the coefficients with 3 decimal digits instead of 8 provides a deviation of only 0.018%, therefore only 3 decimal digits are retained in the table. Although the expression is quite lengthy, its analytical form allows very easy implementation and use in numerical BES and BEHAM programs. Fig. 14b illustrates the proximity of the in-sample CFD simulations (black dots) to the 1:1 line, indicating the very close agreement in line with the high value of R^2.

Fig. 15 and Table 3, Fig. 16 and Table 4, and Fig. 17 and Table 5, provide similar results for the leeward facade, side facade and roof, respectively. High coefficients of determination R^2 are found: 0.9851, 0.9870 and 0.9950. Note that the choice of fourth-order polynomial equations including cross-terms (i.e. terms involving the product of the independent variables) is based on a sensitivity analysis in which polynomials of different orders are evaluated. Ten polynomials are considered: second, third, fourth, fifth and sixth-order polynomials including and excluding cross-terms. The in-sample accuracy of the polynomials is evaluated by comparing the coefficients of determination (R^2). The results are provided in Table 6. It can be seen that fourth, fifth and sixth-order polynomials including cross-terms yield the best performance for all facades (i.e. $R^2 > 0.9850$). As the number of coefficients in a fourth-order polynomial is less than that in a fifth and sixth-order polynomial, in this study fourth-order polynomials are implemented.

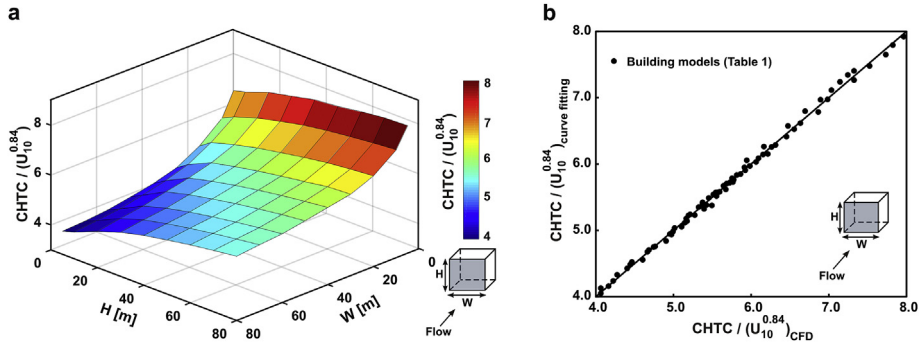

Fig. 14. (a) Forced surface-averaged ratio ($CHTC/U_{10}^{0.84}$) on the windward facade as a function of H and W. (b) Fitted values versus values by CFD: data points used for fit (black dots) for the windward facade.

Table 2
Expression for forced surface-averaged CHTC on the windward facade as a function of reference wind speed U_{10} and building dimensions W and H.

$$CHTC = U_{10}^{0.84}.(a_0 + a_1.W + a_2.W^2 + a_3.W^3 + a_4.W^4 + a_5.H + a_6.H^2 + a_7.H^3 + a_8.H^4 + a_9.W.H + a_{10}.W.H^2 + a_{11}.W.H^3 + a_{12}.W^2.H + a_{13}.W^2.H^2 + a_{14}.W^2.H^3 + a_{15}.W^3.H + a_{16}.W^3.H^2 + a_{17}.W^3.H^3)$$

$a_0 = 7.559$	$a_1 = -2.277E-1$	$a_2 = 6.037E-3$	$a_3 = -7.801E-5$
$a_4 = 3.810E-7$	$a_5 = 4.485E-2$	$a_6 = -8.190E-4$	$a_7 = 1.080E-5$
$a_8 = -6.020E-8$	$a_9 = 1.047E-3$	$a_{10} = -2.430E-5$	$a_{11} = 1.793E-7$
$a_{12} = -3.591E-6$	$a_{13} = 1.385E-7$	$a_{14} = -1.353E-9$	$a_{15} = -9.369E-8$
$a_{16} = 1.757E-9$	$a_{17} = -9.134E-12$		
$R^2 = 0.9977$			

4.3. Relationship between CHTC, reference wind speed and building width and height

Combination of the expressions established in the two sub-sections above yields the CHTC as a trivariate polynomial with U_{10}, W and H as variables. The accuracy of these expressions is evaluated by their application for out-of-sample combinations of (U_{10}, W, H) and comparison with the direct results of the extra CFD simulations (category 3 in Table 1), see Fig. 18. For all combinations, the resulting values of the forced surface-averaged CHTC are also well described by the trivariate polynomials in Tables 2–5. The maximum and average deviations are 6.1% and 3.5% for the

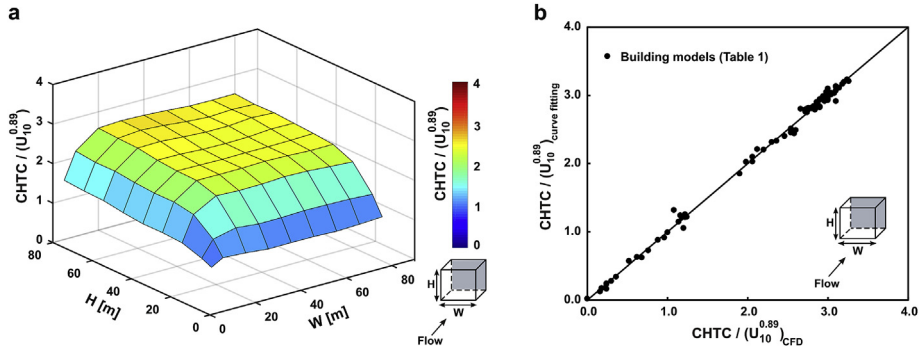

Fig. 15. (a) Forced surface-averaged ratio ($CHTC/U_{10}^{0.89}$) on the leeward facade as a function of H and W. (b) Fitted values versus values by CFD: data points used for fit (black dots) for the leeward facade.

Table 3
Expression for forced surface-averaged CHTC on the leeward facade as a function of reference wind speed U_{10} and building dimensions W and H.

$$CHTC = U_{10}^{0.89}.(a_0 + a_1.W + a_2.W^2 + a_3.W^3 + a_4.W^4 + a_5.H + a_6.H^2 + a_7.H^3 + a_8.H^4 + a_9.W.H + a_{10}.W.H^2 + a_{11}.W.H^3 + a_{12}.W^2.H + a_{13}.W^2.H^2 + a_{14}.W^2.H^3 + a_{15}.W^3.H + a_{16}.W^3.H^2 + a_{17}.W^3.H^3)$$

$a_0 = 3.691E-1$	$a_1 = 5.848E-2$	$a_2 = -3.662E-3$	$a_3 = 6.995E-5$
$a_4 = -4.174E-7$	$a_5 = 5.621E-2$	$a_6 = -2.847E-3$	$a_7 = 5.155E-5$
$a_8 = -3.011E-7$	$a_9 = 7.582E-3$	$a_{10} = -1.455E-4$	$a_{11} = 8.924E-7$
$a_{12} = -1.488E-4$	$a_{13} = 2.751E-6$	$a_{14} = -1.646E-8$	$a_{15} = 8.907E-7$
$a_{16} = -1.569E-8$	$a_{17} = 9.019E-11$		
$R^2 = 0.9851$			

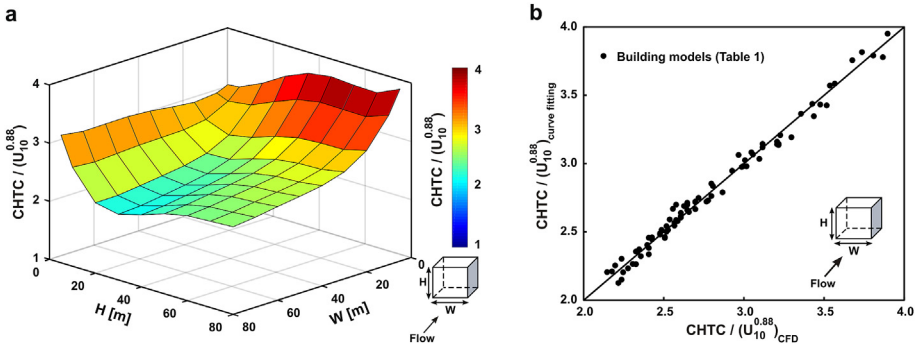

Fig. 16. (a) Forced surface-average ratio CHTC/$U_{10}^{0.88}$ on the side facade as a function of H and W. (b) Fitted values versus values by CFD: data points used for fit (black dots) for the side facade.

Table 4
Expression for forced surface-averaged CHTC on the side facade as a function of reference wind speed U_{10} and building dimensions W and H.

$$CHTC = U_{10}^{0.88}.(a_0 + a_1.W + a_2.W^2 + a_3.W^3 + a_4.W^4 + a_5.H + a_6.H^2 + a_7.H^3 + a_8.H^4 + a_9.W.H + a_{10}.W.H^2 + a_{11}.W.H^3 + a_{12}.W^2.H + a_{13}.W^2.H^2 + a_{14}.W^2.H^3 + a_{15}.W^3.H + a_{16}.W^3.H^2 + a_{17}.W^3.H^3)$$

$a_0 = 3.217$	$a_1 = -4.235E-3$	$a_2 = 1.118E-3$	$a_3 = -2.301E-5$
$a_4 = 1.382E-7$	$a_5 = 6.551E-3$	$a_6 = 1.843E-3$	$a_7 = -4.576E-5$
$a_8 = 3.014E-7$	$a_9 = -6.985E-3$	$a_{10} = 1.402E-4$	$a_{11} = -8.728E-7$
$a_{12} = 1.043E-4$	$a_{13} = -2.052E-6$	$a_{14} = 1.268E-8$	$a_{15} = -5.537E-7$
$a_{16} = 1.070E-8$	$a_{17} = -6.574E-11$		
$R^2 = 0.9870$			

windward facade (Fig. 18a–c), 9.4% and 3.2% for the leeward facade (Fig. 18d–f), 12.9% and 3.9% for the side facade (Fig. 18g–i), 9.4% and 3.2% for the roof (Fig. 18j–l). The related coefficients of determination are 0.9925, 0.9903, 0.9851 and 0.9955, respectively. Given the complexity involved in this study, in spite of some limitations, the in-sample and out-of-sample evaluations provide confidence in the new expressions for the accurate prediction of the CHTC for different buildings.

5. Discussion

This paper has presented a set of four trivariate polynomials expressing the forced CHTC as a function of reference wind speed U_{10} and building width W and height H. Such expressions help in overcoming some the current main limitations associated with existing CHTC expressions. A first main shortcoming is that existing (forced) CHTC expressions focus on wind speed as the main (or

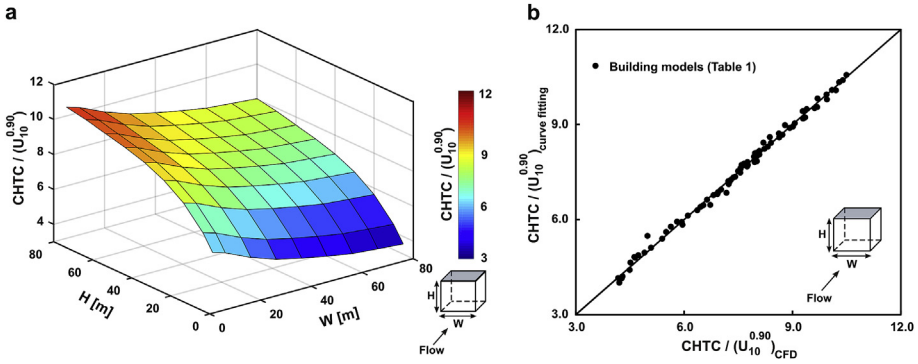

Fig. 17. (a) Surface-averaged ratio (CHTC/$U_{10}^{0.90}$) on the roof as a function of H and W. (b) Fitted values versus values by CFD: data points used for fit (black dots) for the roof.

Table 5
Expression for forced surface-averaged CHTC on the roof as a function of reference wind speed U_{10} and building dimensions W and H.

$$CHTC = U_{10}^{0.90}.(a_0 + a_1.W + a_2.W^2 + a_3.W^3 + a_4.W^4 + a_5.H + a_6.H^2 + a_7.H^3 + a_8.H^4 + a_9.W.H + a_{10}.W.H^2 + a_{11}.W.H^3 + a_{12}.W^2.H + a_{13}.W^2.H^2 + a_{14}.W^2.H^3 + a_{15}.W^3.H + a_{16}.W^3.H^2 + a_{17}.W^3.H^3)$$

$a_0 = 5.383$	$a_1 = -1.320E-1$	$a_2 = 2.211E-3$	$a_3 = -6.099E-6$
$a_4 = -6.369E-8$	$a_5 = 2.320E-1$	$a_6 = -4.653E-3$	$a_7 = 4.830E-5$
$a_8 = -2.004E-7$	$a_9 = 5.224E-3$	$a_{10} = -1.244E-4$	$a_{11} = 9.642E-7$
$a_{12} = -1.643E-4$	$a_{13} = 3.810E-6$	$a_{14} = -2.892E-8$	$a_{15} = 1.115E-6$
$a_{16} = -2.541E-8$	$a_{17} = 1.921E-10$		
$R^2 = 0.9950$			

Table 6
Coefficient of determination (R^2) for in-sample accuracy evaluation of CHTC expressions using different polynomials.

Polynomials	2nd order		3rd order		4th order		5th order		6th order	
	Excluding cross-terms	Including cross-terms	Excluding cross-terms	Including cross-terms	Excluding cross-terms	Including cross-terms	Excluding cross-terms	Including cross-terms	Excluding cross-terms	Including cross-terms
No. of coefficients	4	5	6	10	8	17	10	26	12	37
	0.9689	0.9710	0.9899	0.9923	0.9951	0.9977	0.9964	0.9992	0.9967	0.9995
	0.7940	0.8041	0.9054	0.9380	0.9407	0.9851	0.9471	0.9943	0.9488	0.9966
	0.7382	0.8000	0.8203	0.9445	0.8403	0.9870	0.8427	0.9956	0.8429	0.9977
	0.9789	0.9828	0.9871	0.9920	0.9877	0.9950	0.9878	0.9975	0.9880	0.9990

only) parameter and do not consider the building dimensions or surface width and length as parameters. A second main shortcoming is that most existing CHTC expressions only consider building facades and not building roofs. In addition, facades are generally only classified as either windward or leeward, while flow structures on the side facades and leeward facades can be markedly different. In spite of the large number of CFD simulations made underlying the new expressions, the study contains a number of limitations that provide fertile ground for future research.

The simulations were performed with the 3D steady RANS equations. The validation study has shown that such simulations can accurately reproduce the CHTC at the windward and leeward facade, but less accurately at the side facades and the roof. For all simulations, building depth was fixed and equal to D = 20 m. Especially for the side facades and the roof, and to a lesser extent also for the leeward facade, building depth influences the CHTC and should be considered as a parameter in future extensions of the new expressions. Wind direction was perpendicular to the windward facade, and future research should integrate wind direction in extensions of the new expressions. Furthermore, the validation was performed for a wall-mounted cube in turbulent flow at a Reynolds number of only 4440. While the selection of this validation case was due to the lack of available high-resolution wind-tunnel data of CHTC at realistic Reynolds numbers for building applications (~10^5-10^7), this low Reynolds number does entail limitations. Actually, it is likely that the boundary layers over the model surfaces are mostly laminar [76]. Therefore, further CFD validation studies are required at sufficiently high Reynolds numbers to ensure the turbulent boundary layer is obtained. Future validation studies should also include a larger range of building geometries.

A particular item of concern is surface roughness. All simulations were performed for perfectly smooth buildings surfaces, which is an implicit assumption of low-Re number modeling when the geometry of roughness features is not modeled explicitly. Future work should allow for facade and roof surface roughness to be taken into account in the new expressions.

In this study, the accuracy of the new expressions has been confirmed by in-sample and out-of-sample evaluations that fall within the range of the data for which the CFD simulations have been performed. However, this is not the case for the building dimensions beyond the original data. Therefore, extrapolated results should be treated with caution. Note that the original CFD simulations have been performed for 81 different geometries, with building width (W) and height (H) varying from 5 m to 80 m. Given the typical length scale of buildings (1–100 m), the new expressions therefore cover the majority of buildings.

In spite of these limitations, the new expressions substantially transcend the state of the art, and can easily be implement in Building Energy Simulation programs and BE-HAM (Building Envelope Heat, Air and Moisture transfer) programs.

6. Summary and conclusions

Previous research indicated that the surface-averaged forced convective heat transfer coefficient (CHTC) at a windward building facade can vary substantially as a function of building width and height. However, existing CHTC expressions generally do not consider the building dimensions as parameters and are therefore strictly only applicable for the building geometry for which they were derived. Most CHTC expressions also categorize facades only as either windward or leeward. This indicates the need for new and more generally applicable CHTC expressions. This paper presented new generalized expressions for surface-averaged forced CHTC at building facades and roofs that contain the reference wind speed, the width and the height of the windward building facade as parameters. These expressions were derived from three groups of CFD simulations of wind flow and forced convective heat transfer around 81 different isolated buildings. The 3D Reynolds-averaged Navier-Stokes equations are solved with a combination of the high-Re number realizable k-ε model and the low-Re number Wolfshtein model. First, a validation study was performed with wind-tunnel measurements of surface temperature for a reduced-scale cubic model. Next, the actual simulations were performed on a high-resolution grid with a minimum near-wall cell size of 400 μm to resolve the entire boundary layer, including the viscous sublayer and the buffer layer, which dominate the convective surface resistance. The following conclusions are made:

- The validation study showed that fair to very good agreement can be obtained between the CFD simulations and the wind-tunnel measurements. For the windward surface, the general agreement was very good with average deviations of about 1.7

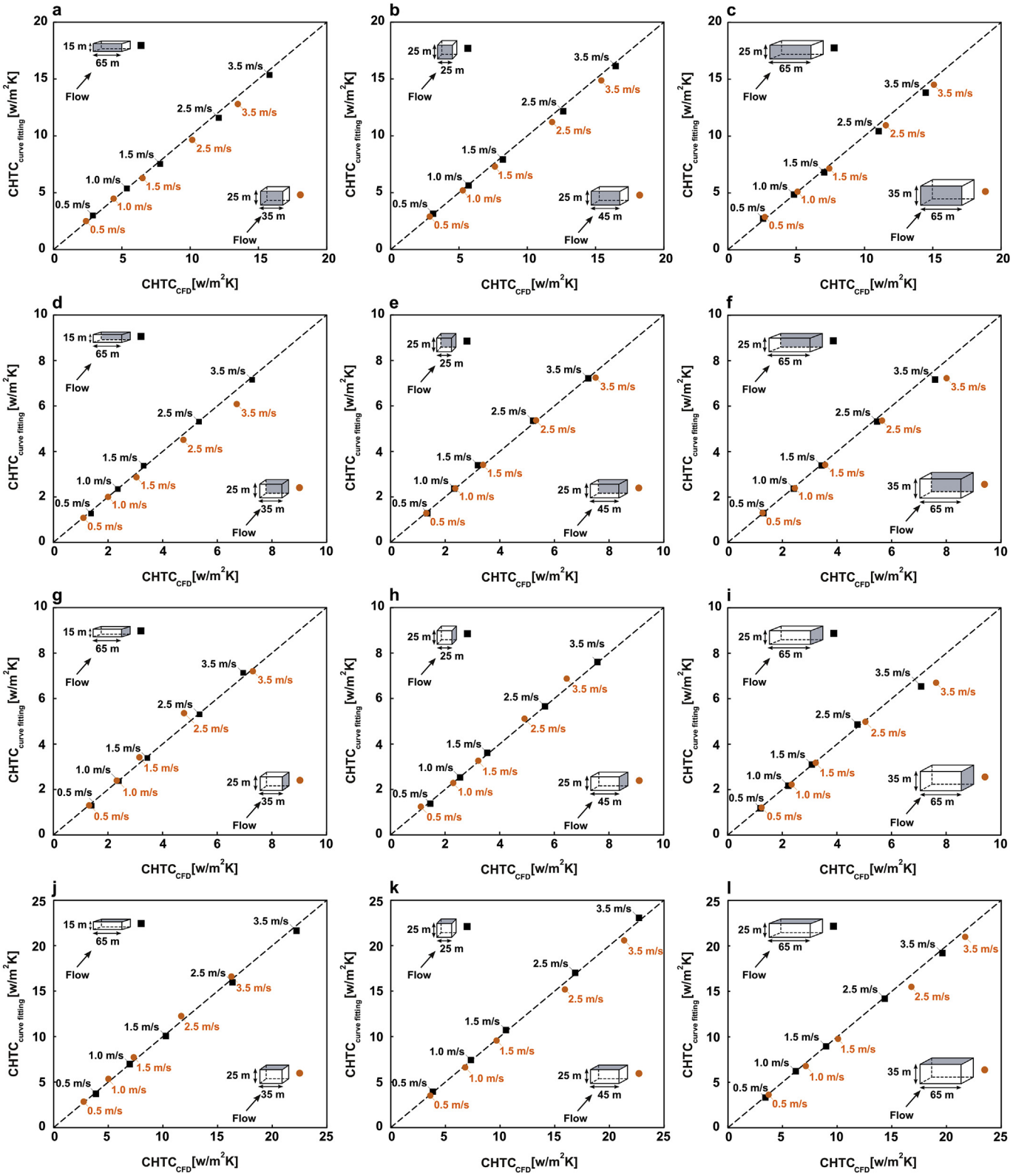

Fig. 18. Out-of-sample evaluation of the expressions for forced CHTC for six building models for U_{10} = 0.5, 1.5, 2.5 and 3.5 m/s: (a–c) windward facade, (d–f) leeward facade, (g–i) side facade, and (j–l) roof.

and 2.4%. Good agreement was obtained for the leeward facade with average deviations of about 3.4 and 2.5%. Less good agreement is present at the top and side surfaces of the cube with average deviations in excess of 6.5 and 6.6%.

- The three groups of simulations around the isolated buildings were performed according to the international best practice guidelines.
- The first group of simulations was performed to establish the expressions of forced surface-averaged CHTC as a function of reference wind speed U_{10} (or Re). The results show that for a given building geometry the relationship between the surface-averaged CHTC and U_{10} is a power law with an exponent α that depends on the type of surface (windward, leeward, side face, roof). This suggests that the establishment of the relationship between CHTC and building width and height should only be performed for a single value of U_{10}, which saved time and computational cost in this study and can do the same in future studies.
- The second group of simulations was performed to establish the expressions of forced surface-averaged CHTC as a function of width and height of windward facade. The results show that the surface-averaged ratio CHTC/U_{10}^{α} for every building surface can be presented with high accuracy by a bivariate polynomial with windward building facade width and height as parameters.
- The third group of simulations was performed to evaluate the out-of-sample accuracy of the expressions, indicating similarly high coefficients of determination as the in-sample evaluation.
- The new CHTC expressions are analytical formulae (trivariate polynomials as a function of U_{10}, windward facade width and building height) that can easily be implemented in Building Energy Simulation programs and Building Envelope Heat-Air-Moisture (BE-HAM) transfer programs.

Acknowledgements

Hamid Montazeri is currently a postdoctoral fellow of the Research Foundation – Flanders (FWO) and is grateful for its financial support (project FWO 12M5316N). The authors gratefully acknowledge the partnership with ANSYS CFD.

References

[1] J.C.R. Hunt, C.J. Abell, J.A. Peterka, H. Woo, Kinematical studies of the flows around free or surface-mounted obstacles; applying topology to flow visualization, J. Fluid Mech. 86 (1978) 179–200.
[2] B. Blocken, T. Stathopoulos, J. Carmeliet, J.L. Hensen, Application of computational fluid dynamics in building performance simulation for the outdoor environment: an overview, J. Build. Perform. Simul. 4 (2011) 157–184.
[3] J.A. Palyvos, A survey of wind convection coefficient correlations for building envelope energy systems' modeling, Appl. Therm. Eng. 28 (2008) 801–808.
[4] M. Mirsadeghi, D. Cóstola, B. Blocken, J.L.M. Hensen, Review of external convective heat transfer coefficient models in building energy simulation programs: implementation and uncertainty, Appl. Therm. Eng. 56 (2013) 134–151.
[5] H.M. Künzel, K. Kiessl, Calculation of heat and moisture transfer in exposed building components, Int. J. Heat. Mass Transf. 40 (1996) 159–167.
[6] H. Janssen, B. Blocken, S. Roels, J. Carmeliet, Wind-driven rain as a boundary condition for HAM simulations: analysis of simplified modelling approaches, Build. Environ. 42 (2007) 1555–1567.
[7] H. Janssen, B. Blocken, J. Carmeliet, Conservative modelling of the moisture and heat transfer in building components under atmospheric excitation, Int. J. Heat. Mass Transf. 50 (2007) 1128–1140.
[8] B. Blocken, S. Roels, J. Carmeliet, A combined CFD–HAM approach for wind-driven rain on building facades, J. Wind Eng. Ind. Aerodyn. 95 (2007) 585–607.
[9] M. Abuku, B. Blocken, S. Roels, Moisture response of building facades to wind-driven rain: field measurements compared with numerical simulations, J. Wind Eng. Ind. Aerodyn. 97 (2009) 197–207.
[10] N. Ito, K. Kimura, J. Oka, Field experiment study on the convective heat transfer coefficient on exterior surface of a building, ASHRAE Trans. 78 (1972) 184–192.
[11] S. Sharples, Full-scale measurements of convective energy losses from exterior building surfaces, Build. Environ. 19 (1984) 31–39.
[12] D.L. Loveday, A.H. Taki, Convective heat transfer coefficients at a plane surface on a full-scale building facade, Int. J. Heat. Mass Transf. 39 (1996) 1729–1742.
[13] Y. Liu, D.J. Harris, Full-scale measurements of convective coefficient on external surface of a low-rise building in sheltered conditions, Build. Environ. 42 (2007) 2718–2736.
[14] A. Hagishima, J. Tanimoto, Field measurements for estimating the convective heat transfer coefficient at building surfaces, Build. Environ. 38 (2003) 873–881.
[15] W. Jürges, Der Wärmeübergang an einer ebenen Wand, Druck und Verlag von R, Oldenbourg, 1924.
[16] E.M. Sparrow, J.W. Ramsey, E.A. Mass, Effect of finite width on heat transfer and fluid flow about an inclined rectangular plate, J. Heat. Transf. 101 (1979) 199–204.
[17] M.K. Chyu, V. Natarajan, Local heat/mass transfer distributions on the surface of a wall-mounted cube, Trans. ASME J. Heat. Transf. 113 (1991) 851–857.
[18] V. Natarajan, M.K. Chyu, Effect of flow angle-of-attack on the local heat/mass transfer from a wall-mounted cube, Trans. ASME J. Heat. Transf. 116 (1994) 552–560.
[19] E.R. Meinders, K. Hanjalic, R.J. Martinuzzi, Experimental study of the local convection heat transfer from a wall-mounted cube in turbulent channel flow, Trans. ASME J. Heat. Transf. 121 (1999) 564–573.
[20] H. Nakamura, T. Igarashi, T. Tsutsui, Local heat transfer around a wall-mounted cube in the turbulent boundary layer, Int. J. Heat. Mass Transf. 44 (2001) 3385–3395.
[21] M.G. Emmel, M.O. Abadie, N. Mendes, New external convective heat transfer coefficient correlations for isolated low-rise buildings, Energy Build. 39 (2007) 335–342.
[22] B. Blocken, T. Defraeye, D. Derome, J. Carmeliet, High-resolution CFD simulations for forced convective heat transfer coefficients at the facade of a low-rise building, Build. Environ. 44 (2009) 2396–2412.
[23] T. Defraeye, B. Blocken, J. Carmeliet, CFD analysis of convective heat transfer at the surfaces of a cube immersed in a turbulent boundary layer, Int. J. Heat. Mass Transf. 53 (2010) 297–308.
[24] P. Karava, C.M. Jubayer, E. Savory, Numerical modelling of forced convective heat transfer from the inclined windward roof of an isolated low-rise building with application to photovoltaic/thermal systems, Appl. Therm. Eng. 31 (2011) 1950–1963.
[25] J. Allegrini, V. Dorer, J. Carmeliet, Analysis of convective heat transfer at building façades in street canyons and its influence on the predictions of space cooling demand in buildings, J. Wind Eng. Ind. Aerodyn. 104 (2012) 464–473.
[26] J. Liu, J. Srebric, N. Yu, Numerical simulation of convective heat transfer coefficients at the external surfaces of building arrays immersed in a turbulent boundary layer, Int. J. Heat. Mass Transf. 61 (2013) 209–225.
[27] J. Liu, M. Heidarinejad, S. Gracik, J. Srebric, The impact of exterior surface convective heat transfer coefficients on the building energy consumption in urban neighborhoods with different plan area densities, Energy Build. 86 (2015) 449–463.
[28] H. Montazeri, B. Blocken, D. Derome, J. Carmeliet, J.L.M. Hensen, CFD analysis of forced convective heat transfer coefficients at windward building facades: influence of building geometry, J. Wind Eng. Ind. Aerodyn. 146 (2015) 102–116.
[29] K.E.A. Ohlsson, R. Östin, T. Olofsson, Accurate and robust measurement of the external convective heat transfer coefficient based on error analysis, Energy Build. 117 (2016) 83–90.
[30] K.E.A. Ohlsson, R. Östin, S. Grundberg, T. Olofsson, Dynamic model for measurement of convective heat transfer coefficient at external building surfaces, J. Build. Eng. 7 (2016) 239–245.
[31] M. Casey, T. Wintergerste, Best Practice Guidelines: ERCOFTAC Special Interest Group on" Quality and Trust in Industrial CFD," ERCOFTAC, 2000.
[32] J. Franke, C. Hirsch, A.G. Jensen, H.W. Krus, M. Schatzmann, P.S. Westbury, S.D. Miles, J.A. Wisse, N.G. Wright, Recommendations on the use of CFD in wind engineering, in: Proc. Int. Conf. Urban Wind Eng. Build. Aerodyn. COST Action C14 Impact Wind Storm City Life Built Environ, Von Karman Institute,Sint-Genesius-Rode, Belgium, 2004.
[33] J. Franke, A. Hellsten, H. Schlünzen, B. Carissimo (Eds.), Best practice guideline for the CFD simulation of flows in the urban environment, COST Office, Brussels, 2007, 3-00-018312-4.
[34] Y. Tominaga, A. Mochida, R. Yoshie, H. Kataoka, T. Nozu, M. Yoshikawa, T. Shirasawa, AIJ guidelines for practical applications of CFD to pedestrian wind environment around buildings, J. Wind Eng. Ind. Aerodyn. 96 (2008) 1749–1761.
[35] J. Franke, A. Hellsten, H. Schlünzen, B. Carissimo, The COST 732 Best Practice Guideline for CFD simulation of flows in the urban environment: a summary, Int. J. Environ. Pollut. 44 (2011) 419–427.
[36] B. Blocken, Computational Fluid Dynamics for urban physics: importance, scales, possibilities, limitations and ten tips and tricks towards accurate and reliable simulations, Build. Environ. 91 (2015) 219–245.
[37] M.A. Leschziner, Computational modelling of complex turbulent flow - expectations, reality and prospects, J. Wind Eng. Ind. Aerodyn. 46 (1993) 37–51.
[38] T. Stathopoulos, Computational wind engineering: past achievements and future challenges, J. Wind Eng. Ind. Aerodyn. 67 (1997) 509–532.
[39] S. Murakami, Current status and future trends in computational wind engineering, J. Wind Eng. Ind. Aerodyn. 67–68 (1997) 3–34.
[40] S. Murakami, Overview of turbulence models applied in CWE–1997, J. Wind

Eng. Ind. Aerodyn. 74–76 (1998) 1–24.
[41] C.J. Baker, Wind engineering—past, present and future, J. Wind Eng. Ind. Aerodyn. 95 (2007) 843–870.
[42] R. Ramponi, B. Blocken, CFD simulation of cross-ventilation for a generic isolated building: impact of computational parameters, Build. Environ. 53 (2012) 34–48.
[43] Y. Tominaga, T. Stathopoulos, CFD simulation of near-field pollutant dispersion in the urban environment: a review of current modeling techniques, Atmos. Environ. 79 (2013) 716–730.
[44] S.D. Sabatino, R. Buccolieri, P. Salizzoni, Recent advancements in numerical modelling of flow and dispersion in urban areas: a short review, Int. J. Environ. Pollut. 52 (2013) 172–191.
[45] B. Blocken, 50 years of computational wind engineering: past, present and future, J. Wind Eng. Ind. Aerodyn. 129 (2014) 69–102.
[46] R.N. Meroney, Ten questions concerning hybrid computational/physical model simulation of wind flow in the built environment, Build. Environ. 96 (2016) 12–21.
[47] Y. Tominaga, T. Stathopoulos, Ten questions concerning modeling of near-field pollutant dispersion in the built environment, Build. Environ. 105 (2016) 390–402.
[48] J.H. Ferziger, Approaches to turbulent flow computation: applications to flow over obstacles, J. Wind Eng. Ind. Aerodyn. 35 (1990) 1–19.
[49] M.A. Leschziner, Modelling engineering flows with Reynolds stress turbulence closure, J. Wind Eng. Ind. Aerodyn. 35 (1990) 21–47.
[50] H. Schlichting, Boundary-layer Theory, sixth ed., McGraw-Hill, 1968.
[51] D.C. Wilcox, Turbulence Modeling for CFD, 1998.
[52] T. Defraeye, B. Blocken, J. Carmeliet, An adjusted temperature wall function for turbulent forced convective heat transfer for bluff bodies in the atmospheric boundary layer, Build. Environ. 46 (2011) 2130–2141.
[53] T. Defraeye, B. Blocken, J. Carmeliet, CFD simulation of heat transfer at surfaces of bluff bodies in turbulent boundary layers: evaluation of a forced-convective temperature wall function for mixed convection, J. Wind Eng. Ind. Aerodyn. 104–106 (2012) 439–446.
[54] J. Allegrini, V. Dorer, T. Defraeye, J. Carmeliet, An adaptive temperature wall function for mixed convective flows at exterior surfaces of buildings in street canyons, Build. Environ. 49 (2012) 55–66.
[55] D.B. Crawley, J.W. Hand, M. Kummert, B.T. Griffith, Contrasting the capabilities of building energy performance simulation programs, Build. Environ. 43 (2008) 661–673.
[56] H.S. Hens, Heat, Air and Moisture Transfer in Insulated Envelope Parts: Task 1, Modelling, Final Report, Acco, Leuven, 1996.
[57] H.S. Hens, Building Physics-heat, Air and Moisture: Fundamentals and Engineering Methods with Examplesand Exercises, John Wiley & Sons, 2012.
[58] C. Hall, W.D. Hoff, Water Transport in Brick, Stone and Concrete, CRC Press, 2011.
[59] G.N. Walton, Passive solar extension of the building loads analysis and system thermodynamics (BLAST) program: Technical Report, United States Army Construction Engineering Research Laboratory, Champaign, IL, 1981.
[60] T.M. McClellan, C.O. Pedersen, Investigation of outside Heat Balance Models for Use in a Heat Balance Cooling Load Calculation Procedure, American Society of Heating, Refrigerating and Air-Conditioning Engineers, Inc., Atlanta, GA (United States), 1997.
[61] B. Blocken, J. Carmeliet, The influence of the wind-blocking effect by a building on its wind-driven rain exposure, J. Wind Eng. Ind. Aerodyn. 94 (2006) 101–127.
[62] B. Blocken, P. Moonen, T. Stathopoulos, J. Carmeliet, Numerical study on the existence of the venturi effect in passages between perpendicular buildings, J. Eng. Mech. 134 (2008) 1021–1028.
[63] B. Blocken, T. Stathopoulos, J. Carmeliet, Wind environmental conditions in passages between two long narrow perpendicular buildings, J. Aerosp. Eng. 21 (2008) 280–287.
[64] B. Blocken, G. Dezsö, J. van Beeck, J. Carmeliet, Comparison of calculation models for wind-driven rain deposition on building facades, Atmos. Environ. 44 (2010) 1714–1725.
[65] E.R. Meinders, Experimental Study of Heat Transfer in Turbulent Flows over Wall Mounted Cubes, PhD thesis, Technische Universiteit Delft, 1998.
[66] B. Blocken, J. Carmeliet, T. Stathopoulos, CFD evaluation of wind speed conditions in passages between parallel buildings—effect of wall-function roughness modifications for the atmospheric boundary layer flow, J. Wind Eng. Ind. Aerodyn. 95 (2007) 941–962.
[67] B. Blocken, T. Stathopoulos, J. Carmeliet, CFD simulation of the atmospheric boundary layer: wall function problems, Atmos. Environ. 41 (2007) 238–252.
[68] T. van Hooff, B. Blocken, Coupled urban wind flow and indoor natural ventilation modelling on a high-resolution grid: a case study for the Amsterdam ArenA stadium, Environ. Model. Softw 25 (2010) 51–65.
[69] Ansys Inc, Ansys Fluent 12.0 – Theory Guide, USA: Lebanon, 2009.
[70] T.-H. Shih, W.W. Liou, A. Shabbir, Z. Yang, J. Zhu, A new k-ε eddy viscosity model for high reynolds number turbulent flows, Comput. Fluids 24 (1995) 227–238.
[71] M. Wolfshtein, The velocity and temperature distribution in one-dimensional flow with turbulence augmentation and pressure gradient, Int. J. Heat. Mass Transf. 12 (1969) 301–318.
[72] S. Murakami, Comparison of various turbulence models applied to a bluff body, J. Wind Eng. Ind. Aerodyn. 46 (1993) 21–36.
[73] W. Rodi, Comparison of LES and RANS calculations of the flow around bluff bodies, J. Wind Eng. Ind. Aerodyn. 69 (1997) 55–75.
[74] Y. Tominaga, A. Mochida, S. Murakami, S. Sawaki, Comparison of various revised k– ε models and LES applied to flow around a high-rise building model with 1: 1: 2 shape placed within the surface boundary layer, J. Wind Eng. Ind. Aerodyn. 96 (2008) 389–411.
[75] J. Wieringa, Updating the Davenport roughness classification, J. Wind Eng. Ind. Aerodyn. 41 (1992) 357–368.
[76] S. Iousef, H. Montazeri, B.J.E. Blocken, P.J.V. van Wesemael, On the use of non-conformal grids for economic LES of wind flow and convective heat transfer for a wall-mounted cube, Build. Environ. 119 (2017) 44–61.